Numerical Calculation of Diffraction Coefficients of Generic Conducting and Dielectric Wedges Using FDTD

Glafkos Stratis, *Member, IEEE*, Veeraraghavan Anantha, and Allen Taflove, *Fellow, IEEE*

***Abstract*— Classical theories such as the uniform geometrical theory of diffraction (UTD) utilize analytical expressions for diffraction coefficient for canonical problems such as the infinite perfectly conducting wedge [1]. In this paper, we present a numerical approach to this problem using the finite-difference time-domain (FDTD) method. We present results for the diffraction coefficient of the two-dimensional (2-D) infinite perfect electrical conductor (PEC) wedge, the 2-D infinite lossless dielectric wedge, and the 2-D infinite lossy dielectric wedge for incident TM and TE polarization and a 90° wedge angle. We compare our FDTD results in the far-field region for the infinite PEC wedge to the well-known analytical solutions obtained using UTD. There is very good agreement between the FDTD and UTD results. The power of this approach using FDTD goes well beyond the simple problems dealt with in this paper. It can, in principle, be extended to calculate diffraction coefficients for a variety of shape and material discontinuities, even in three dimensions.**

***Index Terms*—Electromagnetic scattering, FDTD methods.**

I. Introduction

CLASSICAL theories such as the uniform geometrical theory of diffraction (UTD) utilize analytical expressions for diffraction coefficient for canonical problems such as the infinite perfectly conducting wedge [1]. Although these theories predict the fields accurately in the far-field region for simple problems, it is difficult, if not impossible, to extend them to wedges composed of dielectric and imperfectly conducting materials. In fact, the classical problem of diffraction from an infinite lossless dielectric wedge has not been solved analytically. In this paper, we present a numerical approach using the finite-difference time-domain (FDTD) method [2], [3], which can, in principle, be used to obtain the diffraction coefficients of scatterers of arbitrary shape and composition.

Although FDTD has been proposed recently to numerically determine diffraction coefficients [4] as an alternative to numerous existing methods [5]–[13], this paper follows a different strategy that exploits the temporal causality inherent in FDTD modeling. The proposed method is well applied to straight-wall wedge-type scatterers regardless of the length of the walls. It may not be applicable to curved wedge scatterers where, for example, the time-domain UTD approach [12] is useful.

We first present results for the numerical diffraction coefficient of the two-dimensional (2-D) infinite perfect electrical conductor (PEC) wedge at some representative observation points for incident TM and TE polarization for a given incident angle and a 90° wedge angle. A very good correspondence between these results and the analytical diffraction coefficient in the far-field region indicates the validity of our approach. Then, following the procedure used for the PEC wedge, we compute the numerical diffraction coefficients for the 2-D infinite lossless right-angle dielectric wedge and the 2-D infinite lossy right-angle dielectric wedge for different values of permittivity and conductivity.

II. Description of the Method

In this analysis, we assume that our system is linear. In order to find the diffraction coefficient of a canonical 2-D scatterer for plane wave incidence with either TM or TE polarization, we first find the diffracted impulse response field of the scatterer $h_{\text{num}}(\rho, \phi, t)$ numerically using FDTD. The observation point (ρ, ϕ) and scatterer size is chosen such that the incident, reflected, near-edge diffracted and far-edge diffracted waveforms can be separated out using time-gating. This ensures that the diffracted impulse response $h_{\text{num}}(\rho, \phi, t)$ represents only the effect of diffraction from the desired edge. The Fourier transform of the diffracted impulse response $H_{\text{num}}(\rho, \phi, \omega)$ thus gives the variation of the diffracted field obtained for an unit amplitude plane wave illumination over a wide range of frequencies. The numerical diffraction coefficient D_{num} as a function of frequency and observation position can be found using

$$D_{\text{num}}(\rho, \phi, \omega) = H_{\text{num}}(\rho, \phi, \omega)\sqrt{r}e^{j\beta r} \tag{1}$$

where r is the distance of the observation point from the scattering edge and $\beta = \omega\sqrt{\mu_0\varepsilon_0}$. The Fourier transform has been defined using the $e^{-j\omega t}$ convention. The factor $\sqrt{r}e^{j\beta r}$ in the above equation arises from the nature of the Green's function in two dimensions.

In this analysis, we can also find the diffracted field for an arbitrary incident wave (TM or TE polarized) as a function of time and observation position by convolving $h_{\text{num}}(\rho, \phi, t)$ with the time history of the incident wave. If the observation point for a scatterer is such that the incident, reflected, and

Manuscript received June 21, 1996; revised February 15, 1997.

G. Stratis and V. Anantha are with the Cellular Infrastructure Group, Motorola Inc., Rolling Meadows, IL 60008 USA.

A. Taflove is with the Electrical and Computer Engineering Department, McCormick School of Engineering, Northwestern University, Evanston, IL 60208 USA.

Publisher Item Identifier S 0018-926X(97)07222-0.

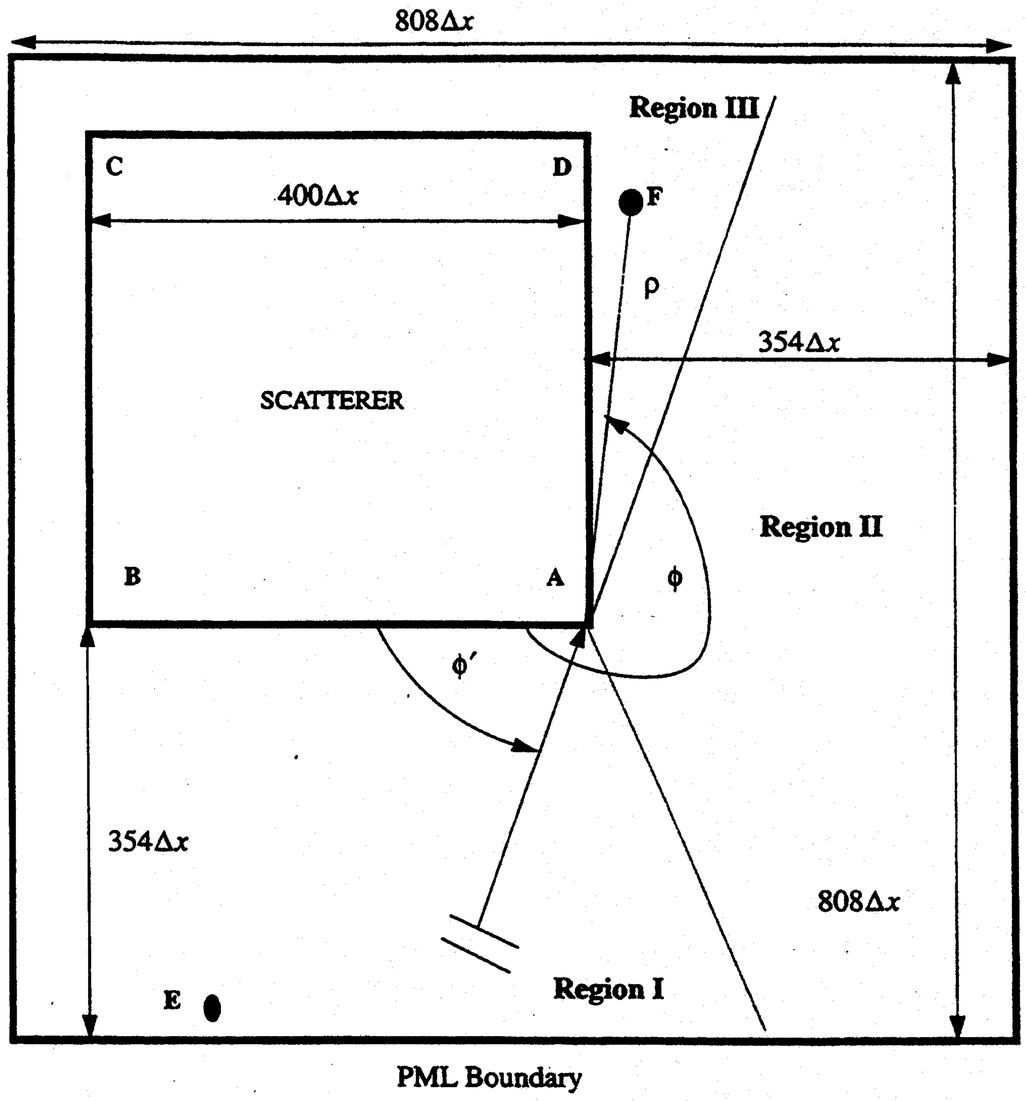

Fig. 1. Two-dimensional geometry of the grid and scatterer.

diffracted fields cannot be separated in time, the incident or reflected fields can be found and subtracted from the total field, and the diffraction coefficients can be calculated as described above.

III. Diffraction Coefficient for PEC Wedge

We apply the general approach outlined above to numerically determine the diffraction coefficient of the PEC wedge with a 90° wedge angle. The 2-D geometry of the grid and square-wedge scatterer is shown in Fig. 1. Vertex A in the figure is shown as the scattering edge and is hence chosen to be the origin of the cylindrical coordinate system used for the calculation of the diffraction coefficient. The infinite extent of the scattering wedge in the horizontal plane is simulated by choosing the side length of the square scatterer to be such that for the incident angles and observation points considered, the diffracted field from edge A can be causally separated from the incident and reflected fields (if present) and from the diffracted fields of the other vertices. The observation point can be thought of as being in one of the three regions shown in Fig. 1: Region I (incident, reflected, and diffracted fields present), Region II (incident and diffracted fields only), and Region III (diffracted field only).

The incident illumination (Fig. 2) is a pulsed plane wave of center frequency 850 MHz and a Gaussian envelope of 1.3-ns duration (full width at half maximum). This wave effectively simulates an unnormalized pseudo delta function and has substantial spectral content from 300 MHz to 1.3 GHz. For the TM (TE) polarized incident wave, an electric- (magnetic-) field source $X_{\text{inc}}(t)$ is used and the diffracted electric (magnetic) field $X_{\text{dif}}(\rho, \phi, t)$ is computed at representative points in Regions I, II, and III for various angles of illumination using a 2-D FDTD code with Berenger perfectly matched layer (PML)

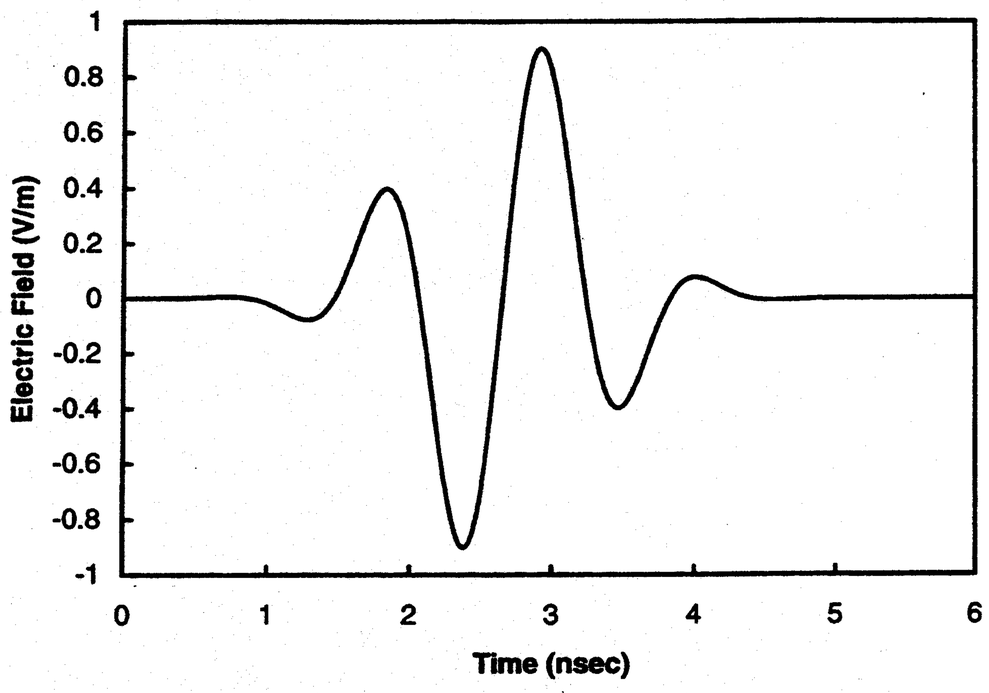

Fig. 2. Electric field source for the TM polarization case. Pulsed plane wave with a Gaussian envelope of 1.3-ns duration full width at half maximum (FWHM).

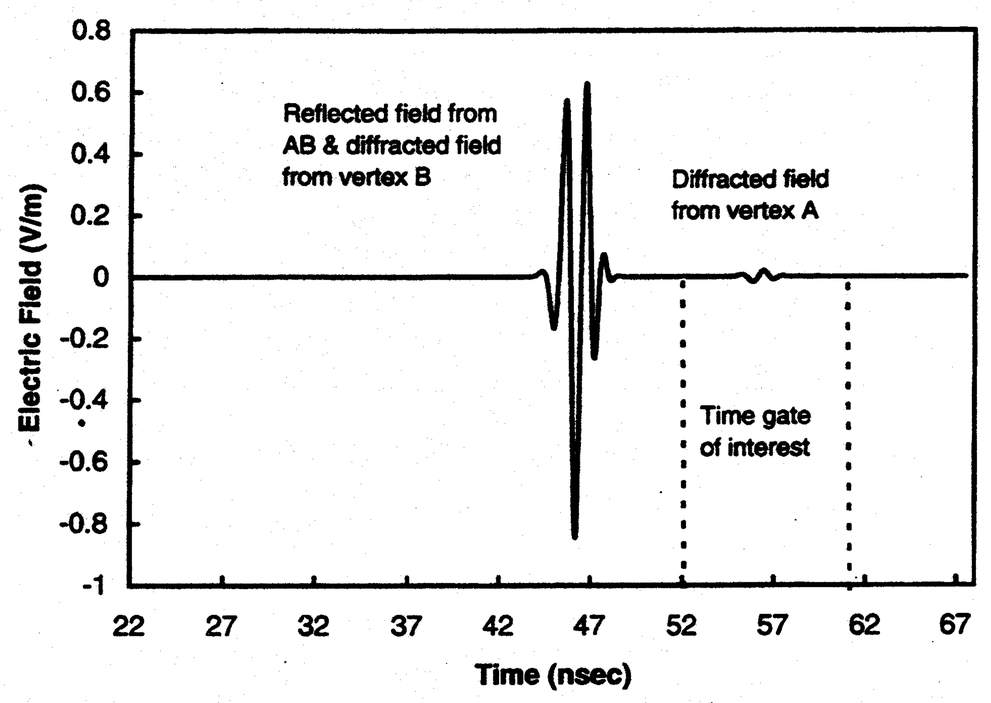

Fig. 3. Time variation of electric field scattered from PEC wedge for the TM polarization case at observation point E ($\rho = 8.32$ m, $\phi = 49.56°$). Diffracted field from vertex A is separated in time from the other fields.

[14] absorbing boundary condition. In the FDTD code, we use square grid cells of side length of resolution $\lambda_0/20$ or smaller to minimize numerical errors, where λ_0 is the wavelength at 850 MHz. Since the incident illumination $X_{\text{inc}}(\rho, \phi, t)$ is unnormalized, the Fourier transform of the diffracted field impulse response $H_{\text{num}}(\rho, \phi, \omega)$ is given by

$$H_{\text{num}}(\rho, \phi, \omega) = \frac{\mathcal{F}\{X_{\text{dif}}(\rho, \phi, t)\}}{\mathcal{F}\{X_{\text{inc}}(0, \phi, t)\}}. \tag{2}$$

Thus, the numerical diffraction coefficient D_{num} from (1) is given by

$$D_{\text{num}}(\rho, \phi, \omega) = \frac{\mathcal{F}\{X_{\text{dif}}(\rho, \phi, t)\}}{\mathcal{F}\{X_{\text{inc}}(0, \phi, t)\}} \sqrt{\rho} e^{j\beta\rho} \tag{3}$$

where ρ is the distance of the observation point from the scattering edge.

We compare our FDTD results in the far-field region for the infinite PEC wedge to the well-known analytical solutions obtained using UTD. References [1] and [15] provide asymptotic analytical expressions for the diffraction coefficient as a function of the positions of the source and the observation points and the wave frequency. The diffraction coefficient D_s

for TM (soft) polarization and the diffraction coefficient D_h for TE (hard) polarization are given by

$$D_s(\rho,\phi,\phi',\omega) = \frac{-e^{-j\pi/4}}{2n\sqrt{2\pi\beta}}\left[\left(\cot\left(\frac{\pi+\xi^-}{2n}\right)F(\beta,\rho,g^+(\xi^-))\right.\right.$$
$$+\cot\left(\frac{\pi-\xi^-}{2n}\right)F(\beta,\rho,g^-(\xi^-))\Big)$$
$$-\left(\cot\left(\frac{\pi+\xi^+}{2n}\right)F(\beta,\rho,g^+(\xi^+))\right.$$
$$\left.\left.+\cot\left(\frac{\pi-\xi^+}{2n}\right)F(\beta,\rho,g^-(\xi^+))\right)\right] \quad (4)$$

$$D_h(\rho,\phi,\phi',\omega) = \frac{-e^{-j\pi/4}}{2n\sqrt{2\pi\beta}}\left[\left(\cot\left(\frac{\pi+\xi^-}{2n}\right)F(\beta,\rho,g^+(\xi^-))\right.\right.$$
$$+\cot\left(\frac{\pi-\xi^-}{2n}\right)F(\beta,\rho,g^-(\xi^-))\Big)$$
$$+\left(\cot\left(\frac{\pi+\xi^+}{2n}\right)F(\beta,\rho,g^+(\xi^+))\right.$$
$$\left.\left.+\cot\left(\frac{\pi-\xi^+}{2n}\right)F(\beta,\rho,g^-(\xi^+))\right)\right] \quad (5)$$

where $\xi^+ = \phi + \phi'$, $\xi^- = \phi - \phi'$, the wedge factor $n = 1.5$ for a right-angle wedge, and $F(X)$ is the Fresnel's transition function given by

$$F(X) = 2j\sqrt{X}e^{jX}\int_{\sqrt{X}}^{\infty} e^{-j\tau^2}\,d\tau. \quad (6)$$

We used the FORTRAN computer program presented in [15] and [16] to compute the diffraction coefficients described above as a function of frequency. To compute Fresnel's transition function, the following asymptotic expressions (for large and small arguments) were used:

$$F(X) \approx \left(\sqrt{\pi X} - 2Xe^{j\pi/4} - \frac{2}{3}X^2e^{-j\pi/4}\right)e^{j(\pi/4+X)} \quad (\text{for } X < 0.3) \quad (7a)$$

$$F(X) \approx 1 + \mathbf{j}\frac{1}{2X} - \frac{3}{4X^2} - \mathbf{j}\frac{15}{8X^3} + \frac{75}{16X^4} \quad (\text{for } X > 5.5). \quad (7b)$$

For intermediate arguments, a linear interpolation was used to calculate this function.

We now present results for the diffraction coefficient at two representative observation points shown in Fig. 1: point E ($\rho = 8.32$ m, $\phi = 49.56°$) in Region 1 and point F ($\rho = 6.30$ m, $\phi = 262.37°$) in Region 3. The plane wave excitation is a TE or TM polarized incident wave with $\phi' = 80°$. Fig. 3 shows the time variation of the total electric field at point E for the TM case. This figure illustrates the procedure of time-gating to extract the diffracted electric field $X_{\text{dif}}(\rho,\phi,t)$. We compare the amplitude of the diffraction coefficient obtained as a function of frequency using FDTD and (4)–(6) at observation point E in Fig. 4 and F in Fig. 5. There is very good agreement to within 1% in the frequency range 30 MHz to 1.3 GHz of the asymptotic and FDTD results. Additional studies have shown exactly the same level of agreement in Region II where only the incident and diffracted fields are present. Our numerical experiments have shown that the TE case requires slightly higher FDTD grid resolution than the TM case to achieve approximately the same accuracy for the same geometry at 850 MHz ($\lambda_0/25$ as opposed to $\lambda_0/20$). This is in spite of the theory [17] that shows that the numerical dispersion properties of the TE and the TM grids are identical for the same grid resolution. This interesting observation is currently being studied by our group. We speculate that diffracted waves generated for the TE case have more sensitive phase characteristics than those generated for the TM case.

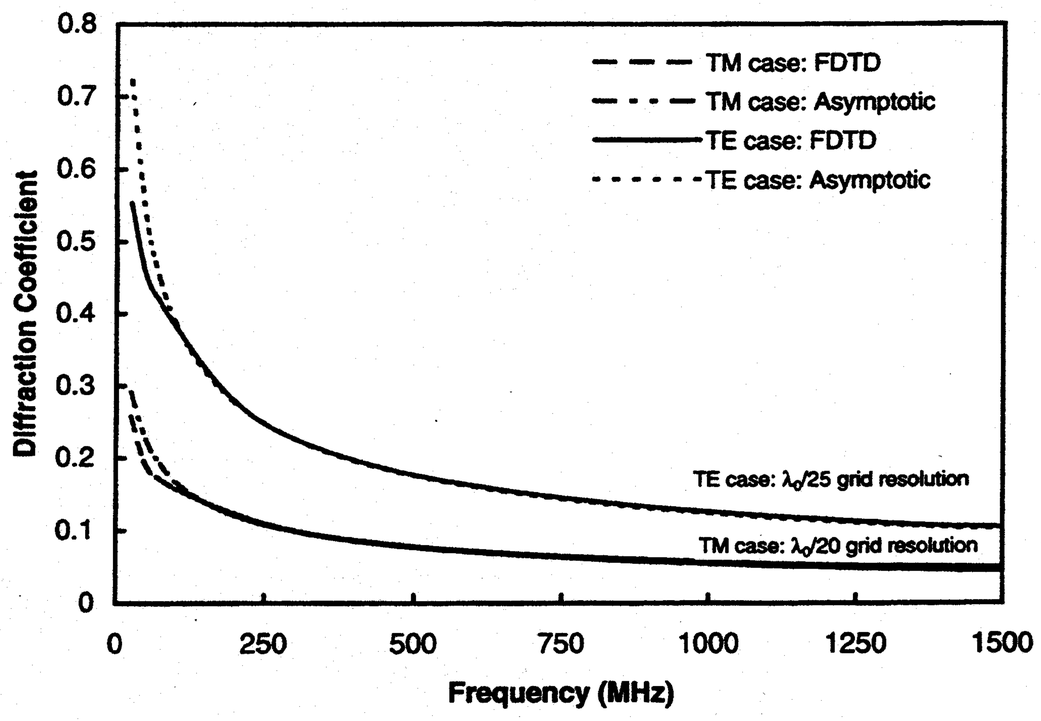

Fig. 4. Comparison of the asymptotic and FDTD results for the diffraction coefficient for PEC wedge at observation point E ($\rho = 8.32$ m, $\phi = 49.56°$) in Region I for TE ($\lambda_0/25$ grid resolution), and TM ($\lambda_0/20$ grid resolution) polarizations.

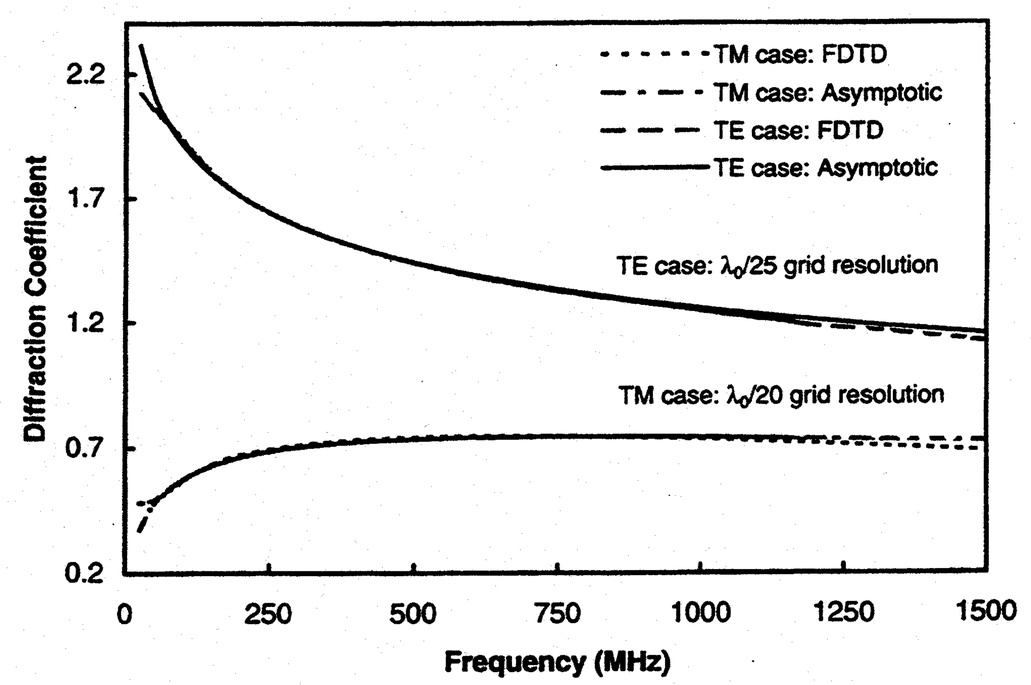

Fig. 5. Comparison of the asymptotic and FDTD results for the diffraction coefficient for PEC wedge at observation point F ($\rho = 6.30$ m, $\phi = 262.37°$) in Region III for TE ($\lambda_0/25$ grid resolution), and TM ($\lambda_0/20$ grid resolution) polarizations.

IV. Diffraction Coefficient for Infinite Dielectric Wedges

We apply the numerical method using FDTD described above to determine the diffraction coefficient for infinite lossless and lossy dielectric wedges with a 90° wedge angle for TM and TE polarization. We modify the 2-D FDTD codes used for the PEC wedge by changing the material properties of the scatterer. For plane wave incident illumination (Fig. 2)

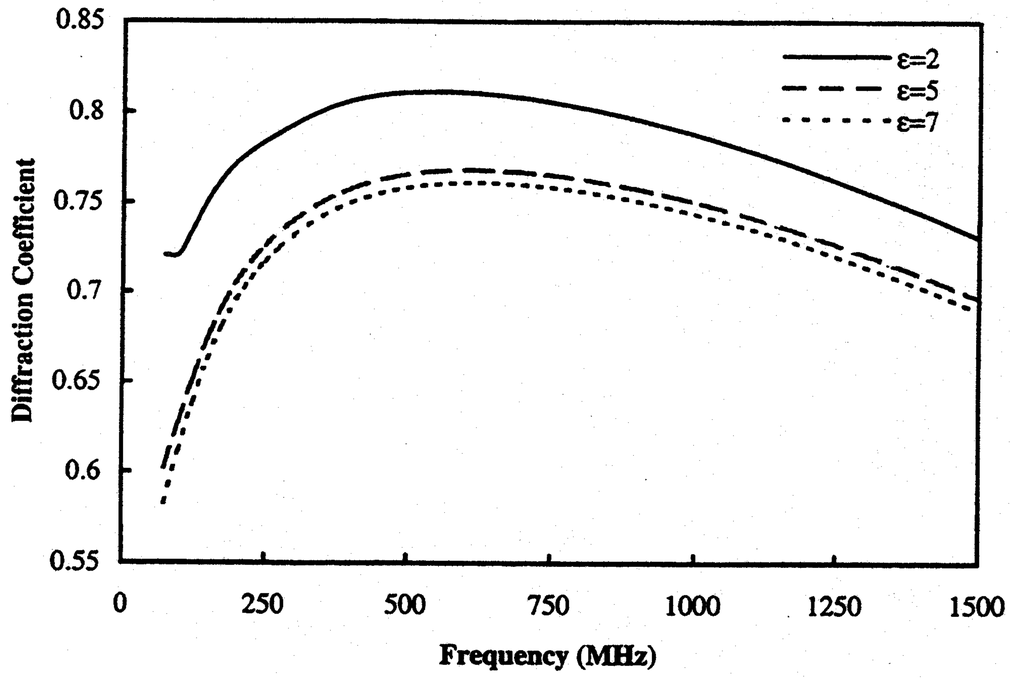

Fig. 6. FDTD computed diffraction coefficient for infinite lossless dielectric wedge at observation point F ($\rho = 6.30$ m, $\phi = 262.37°$) for the TM polarization case. Results are shown for $\varepsilon = 2$, $\varepsilon = 5$, $\varepsilon = 7$ for a fixed-grid resolution $\lambda_0/20$.

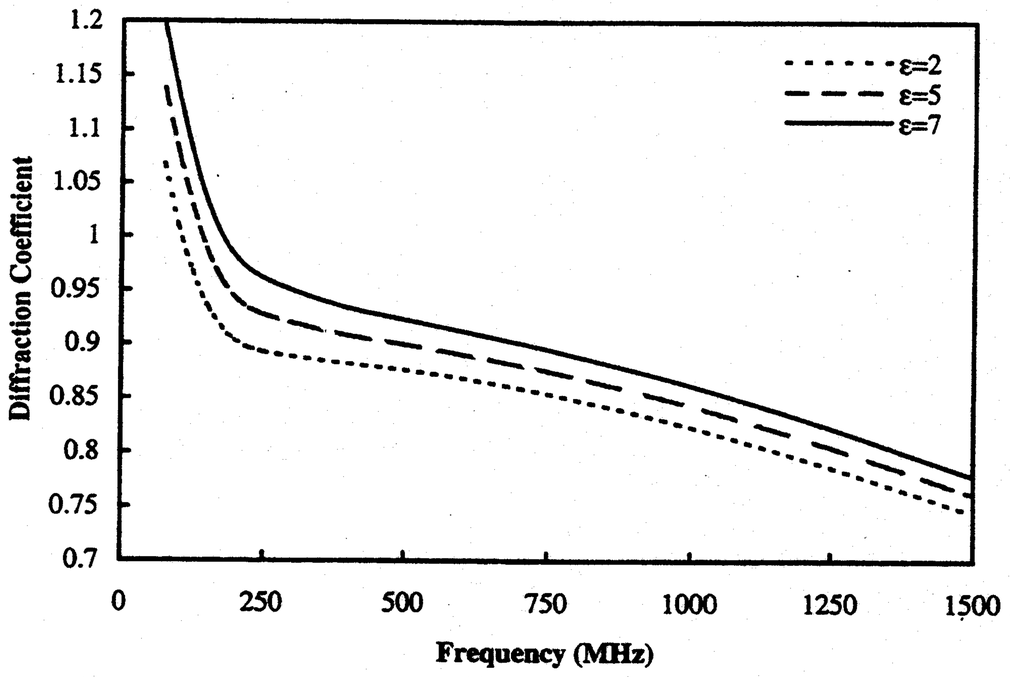

Fig. 7. FDTD computed diffraction coefficient for infinite lossless dielectric wedge at observation point F ($\rho = 6.30$ m, $\phi = 262.37°$) for the TE polarization case. Results are shown for $\varepsilon = 2$, $\varepsilon = 5$, $\varepsilon = 7$ for a fixed-grid resolution $\lambda_0/20$.

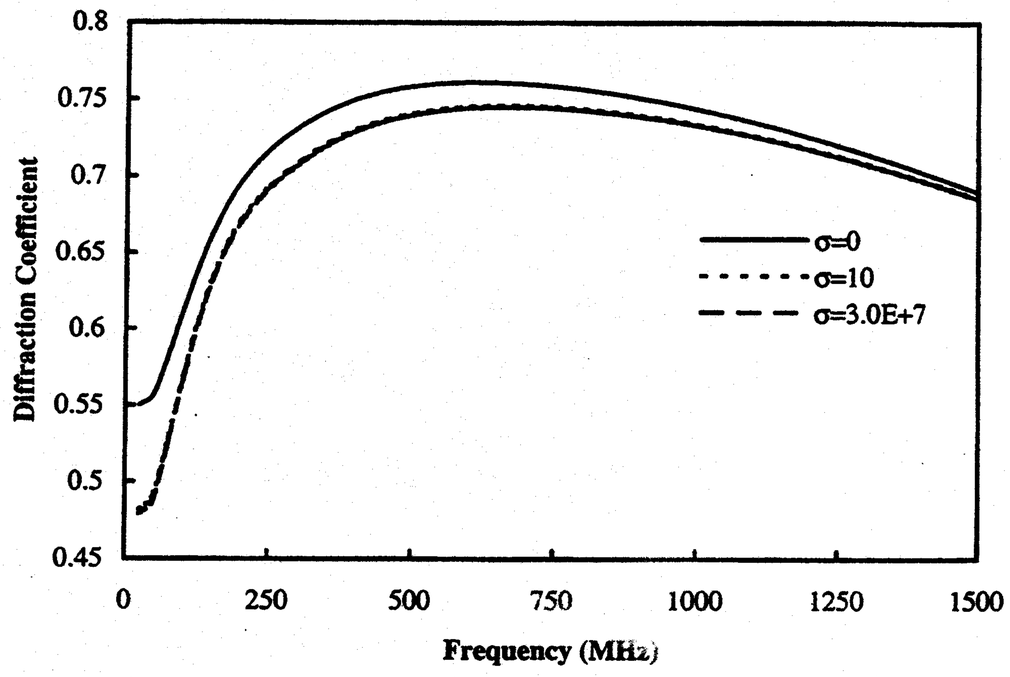

Fig. 8. FDTD computed diffraction coefficient for infinite dielectric wedge at observation point F ($\rho = 6.30$ m, $\phi = 262.37°$) for the TM polarization case. Results are shown for fixed dielectric constant ($\varepsilon = 7$) and varying conductivity for a fixed-grid resolution $\lambda_0/20$.

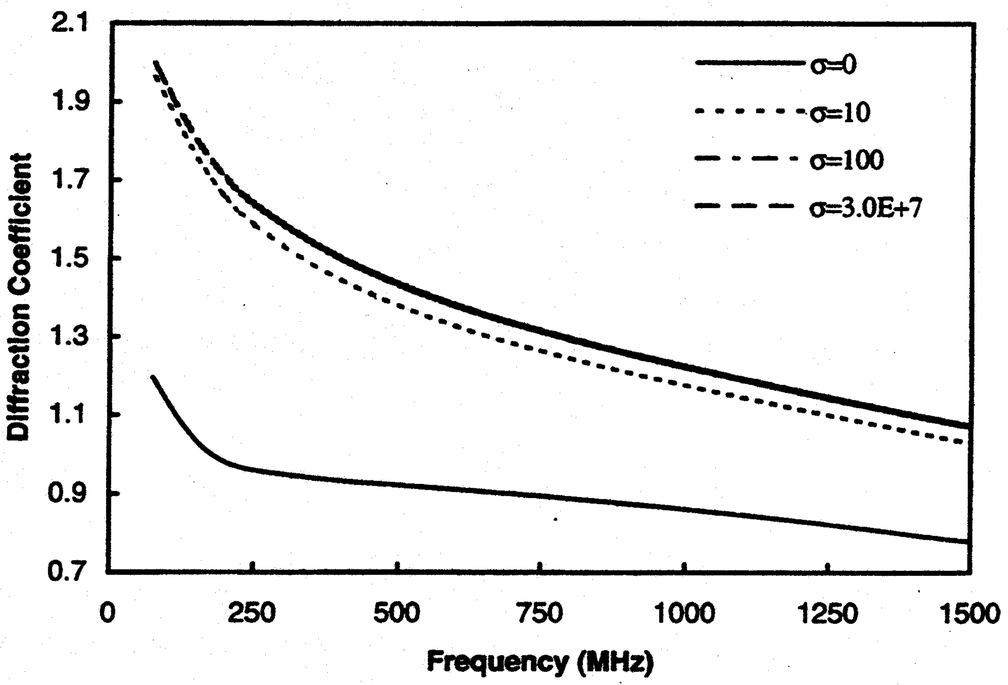

Fig. 9. FDTD computed diffraction coefficient for infinite dielectric wedge at observation point F ($\rho = 6.30$ m, $\phi = 262.37°$) for the TE polarization case. Results are shown for fixed dielectric constant ($\varepsilon = 7$) and varying conductivity for a fixed-grid resolution $\lambda_0/20$.

with the time dependence $X_{\text{inc}}(t)$, the total fields are computed using FDTD at various representative observation points. We present results for the diffraction coefficient at observation point F which is in the forward scattering region and is of practical interest for diffraction problems. For simplicity, the plane wave illumination angle ($\phi' = 80°$) and the material are chosen such that the refracted wave inside the dielectric undergoes total internal reflection from face AD of the wedge, shown in Fig. 1. This ensures that the transmitted fields through the dielectric do not reach point F, allowing us to easily find $X_{\text{dif}}(\rho, \phi, t)$ using time gating. For a general case where the refracted wave cannot be eliminated using total internal reflection, the diffraction coefficient can be calculated by first subtracting the transmitted field (which can be found analytically) from the total field. Figs. 6 and 7 show the variation of the amplitude of the diffraction coefficient at observation point F as a function of frequency for TM and TE polarization, respectively, for selected lossless dielectric parameters. The grid resolution is fixed at $\lambda_0/20$ for each case.

Figs. 8 and 9 show the variation of the amplitude of the diffraction coefficient at observation point F as a function of frequency for TM and TE polarization, respectively, for selected lossy dielectric parameters. The permittivity is kept fixed ($\varepsilon = 7$), while the conductivity is varied from zero (lossless case) to a very large value (metal). As expected, Figs. 8 and 9 indicate that as the conductivity is increased, the diffraction coefficient converges to the value obtained for the PEC wedge.

V. Conclusion

In this paper, we presented a numerical approach using the FDTD method to obtain diffraction coefficients for scatterers in two dimensions. We illustrated the accuracy of this method for an infinite right-angle 2-D PEC wedge for selected key observation regions, and extended the method to infinite right-angle lossless and lossy dielectric wedges.

In principle, this method can be extended to calculate diffraction coefficients of generic wedges with arbitrary wedge angles using the contour-path FDTD approach described in [18]. Further, the diffraction coefficient can be found at any far-field observation position since the contributions of the incident, reflected, and transmitted fields to the total field can

be determined (numerically or theoretically) and subtracted from the total field. Also, the near- to far-field transformations described in [19] can be used to find the diffraction coefficients at any distance away from the scatterer using the numerical fields obtained near the scatterer.

A desirable goal of this research is to calculate a library of numerical diffraction coefficients for a variety of shape and material discontinuities, even in three dimensions. For the most interesting practical applications, i.e., observation points in far-field shadow regions, the assumption of $1/\sqrt{r}$ behavior of the diffracted field holds and the library/table of diffraction coefficients could be a function of angle only. It is to this practical engineering case that we aim this approach. In combination with ray-tracing software, this could be valuable in the accurate estimation of the propagation of electromagnetic fields in an urban environment, a problem that is especially interesting to the cellular and personal communications industry.

REFERENCES

[1] R. G. Kouyoumjian and P. H. Pathak, "A uniform geometrical theory of diffraction for an edge in perfectly conducting surface," *Proc. IEEE*, vol. 62, pp. 1448–1461, Nov. 1974.

[2] K. S. Yee, "Numerical solution of initial boundary value problems involving Maxwell's equations in isotropic media," *IEEE Trans. Antennas Propagat.*, vol. AP-14, pp. 302–307, May 1966.

[3] A. Taflove and M. E. Brodwin, "Numerical solution of steady state electromagnetic scattering problems using the time-dependent Maxwell's equations," *IEEE Trans. Microwave Theory Tech.*, vol. MTT-23, pp. 623–630, Aug. 1975.

[4] D. Ge and Z. Zhu, "Numerical calculation of diffraction coefficient for conducting edge coated by absorbing material," *Acta Electron. Sinica*, vol. 24, no. 3, pp. 27–31, 1996.

[5] G. F. Herrmann, "Numerical computation of diffraction coefficients," *IEEE Trans. Antennas Propagat.*, vol. AP-35, pp. 53–61, Jan. 1987.

[6] G. F. Herrmann and S. M. Strain, "Numerical diffraction coefficients in the shadow transition region," *IEEE Trans. Antennas Propagat.*, vol. 36, pp. 1244–1251, Sept. 1988.

[7] H. J. Bilow, "Scattering by an infinite wedge tensor impedance boundary conditions—A moment/physical optics solution for the currents," *IEEE Trans. Antennas Propagat.*, vol. 39, pp. 767–773, June 1991.

[8] M. P. Hurst, "Improved numerical diffraction coefficients with application to frequency-selective surfaces," *IEEE Trans. Antennas Propagat.*, vol. 40, pp. 606–612, June 1992.

[9] ———, "Numerical diffraction coefficients for surface waves," *IEEE Trans. Antennas Propagat.*, vol. 41, pp. 458–464, Apr. 1993.

[10] N. Y. Zhu and F. M. Landstorfer, "Numerical determination of diffraction slope and multiple-diffraction coefficients of impedance wedges by the method of parabolic equation: Space waves," *IEEE Trans. Antennas Propagat.*, vol. 43, pp. 1429–1435, Dec. 1995.

[11] G. Pelosi, S. Selleri, and R. D. Graglia, "The parabolic equation model for the numerical analysis of the diffraction at an impedance wedge: Skew incidence case," *IEEE Trans. Antennas Propagat.*, vol. 44, pp. 267–268, Feb. 1996.

[12] P. R. Rousseau and P. H. Pathak, "Time-domain uniform geometrical theory of diffraction for a curved wedge," *IEEE Trans. Antennas Propagat.*, vol. 43, pp. 1375–1382, Dec. 1995.

[13] P. H. Pathak, "Techniques for high-frequency problems," in *Antenna Handbook: Theory, Applications, and Design*, Y. T. Lo and S. W. Lee, Eds. New York: Van Nostrand Reinhold, 1988, ch. 4.

[14] J. P. Berenger, "A perfectly matched layer for the absorption of electromagnetic waves," *J. Computat. Phys.*, vol. 114, pp. 185–200, 1994.

[15] C. A. Balanis, "Geometrical theory of diffraction," in *Advanced Engineering Electromagnetics*. New York: Wiley, 1989, ch. 13.

[16] "The modern geometrical theory of diffraction," *Short Course Notes*, Electrosci. Lab., Ohio State Univ., 1985, vol. 1.

[17] A. Taflove, *Computational Electrodynamics: The Finite-Difference Time-Domain Method*. Boston, MA: Artech House, 1995, pp. 93–105.

[18] *Ibid*, pp. 292–304.

[19] *Ibid*, pp. 203–224.

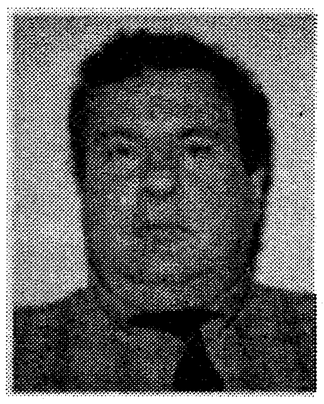

Glafkos Stratis (M'96) received the M.Sc. degree in electrical engineering from the University of Illinois at Chicago (specializing in nonlinear optics), in 1990.

He entered the Ph.D. program at University of Illinois at Chicago after 1990 where he worked as a Research Assistant until 1992. He then joined Motorola Inc., Rolling Meadows, IL, where he is working on wave propagation and simulations. He is currently a Lead Engineer with the NETPLAN Group (Motorola's RF propagation tool group). His research interests include wave propagation and scattering in complex media, numerical methods in electromagnetics, antennas, remote sensing, and nonlinear optics.

Veeraraghavan Anantha received the B.Tech degree in engineering physics from the Indian Institute of Technology, Bombay, India, in 1994, and the M.S. degree in physics from Northwestern University, Evanston, IL, in 1996.

From 1995 to 1996, he was a Research Assistant in the Department of Electrical Engineering, Northwestern University, Evanston, IL, where he worked on electromagnetic scattering problems using numerical methods. He is currently working as an RF engineer at the Cellular Infrastructure Group, Motorola Inc., Rolling Meadows, IL. His current research interests include propagation studies for wireless communications and computational electrodynamics.

Allen Taflove (M'75–SM'84–F'90), for photograph and biography, see p. 374 of the March 1997 issue of this TRANSACTIONS.